Photochemical & Photobiological Sciences

Accepted Manuscript

This is an *Accepted Manuscript*, which has been through the Royal Society of Chemistry peer review process and has been accepted for publication.

Accepted Manuscripts are published online shortly after acceptance, before technical editing, formatting and proof reading. Using this free service, authors can make their results available to the community, in citable form, before we publish the edited article. We will replace this *Accepted Manuscript* with the edited and formatted *Advance Article* as soon as it is available.

You can find more information about *Accepted Manuscripts* in the Information for Authors.

Please note that technical editing may introduce minor changes to the text and/or graphics, which may alter content. The journal's standard Terms & Conditions and the Ethical guidelines still apply. In no event shall the Royal Society of Chemistry be held responsible for any errors or omissions in this *Accepted Manuscript* or any consequences arising from the use of any information it contains.

ROYAL SOCIETY OF CHEMISTRY

www.rsc.org/pps

Photochemical & Photobiological Sciences

Cite this: DOI: 10.1039/c0xx00000x

www.rsc.org/xxxxxx

In Vitro Activity Studies of Hyperthermal Near-Infrared NanoGUMBOS in MDA-MB-231 Breast Cancer Cells

Jonathan C. Dumke,[a] Ammar Qureshi,[b] Suzana Hamdan,[a] Kresimir Rupnik,[a] Bilal El-Zahab,[a,§] Daniel J. Hayes,[b] and Isiah M. Warner*[,a]

Abstract

A new kind of material called nanoGUMBOS, comprised entirely of cations and anions have been developed by pairing various functional ions that afford fluorescent activity with biocompatible ions, in a process very much akin to that employed in ionic liquid chemistry. In the present study, spectral and biological properties of NIR absorbing nanoGUMBOS were evaluated using electron microscopy, dynamic light scattering, absorbance, thermal imaging, and live/dead fluorescence assays in conjunction with malignant MDA-MB-231 and non-malignant HS-578-BST epithelial human breast cells. The primary focus of this study was to maximize heat generation using NIR laser irradiation and minimize non-specific cytotoxicity by using biocompatible constituent ions (e.g. amino acids, vitamins, or organic acids). Concurrently, in order to generate highly responsive nanomaterials for NIR-laser-triggered hyperthermia, optimization of nanoparticle size, shape, and uniformity were investigated. Evaluation of data from hyperthermal studies of NIR absorbing nanoGUMBOS shows that these materials can achieve temperatures above the threshold for killing cancerous cells. Additionally, *in vitro* cell based assays demonstrate promising hyperthermal effects in cancer derived epithelial cells.

Introduction

The American Cancer Society estimates that more than 1.5 million new cases of cancer will be recorded by the end of 2014.[1] Fortunately, early detection and treatment of cancers have reduced the mortality rate over the past several decades.[2] One of the oldest therapeutics for cancer treatment, dating back to antiquity, is the use of cauterization, or heat.[3] The application of heat to kill cancer cells can be made less invasive by using photothermal nanoparticles activated by radiowaves,[4] microwaves,[5-7] magnetic field,[8-10] or near infrared laser.[11-13] In this regard, nanoparticles such as gold[14-18] and porphysomes[19] when subjected to near-infrared (NIR) laser light have been shown to provide sufficient thermal energy to raise intracellular temperature above the threshold of 42 – 45 °C and initiate cancer cell apoptosis or necrosis.[20, 21] NIR laser irradiation is attractive for use *in vivo* for photothermal activation as the human tissue has an absorption minima in the wavelength range of 750 – 1100 nm allowing for maximum photon penetration depth.[22, 23]

Several previously described cancer therapeutic nanoparticles have conjugated folate molecules on the surface to enhance selectivity toward cancer cells.[24-26] Folate (or vitamin B_9) is used to synthesize DNA, repair DNA, and hence is critical for cell proliferation.[27] As cancer cells divide rapidly requiring large amounts of folate, there is an overexpression of the folate-receptor alpha proteins in the cancerous cell membrane.[28] An over abundance of folate-receptor alpha proteins has been found on brain, ovarian, breast, kidney, colon, renal, and lung cancer cells suggesting that folate selectivity may have broad application for the treatment of cancers.[27, 29] Many of the aforementioned hyperthermal materials (i.e. gold and porphysomes) require extensive syntheses to improve biocompatibility and into nanoparticles.

A new class of nanoparticles has been derived from a ***g***roup of ***u***niform ***m***aterials ***b***ased on ***o***rganic ***s***alts (GUMBOS). GUMBOS have a unique set of properties such as limited volatility, variable viscosity and solubility, melting point range of 25 – 250 °C, and primarily exist in the solid state. GUMBOS are designed to be task-specific similar to ionic liquids with substantial flexibility to tune properties. In addition, by implementation of a simple metathesis reaction, the cation and/or anion species can afford fluorescence,[30-33] magnetic,[33-35] chiral selectivity,[32, 35, 36] photothermal,[37] chemotherapeutic,[38] and antibiotic properties.[39] These facile tunable compounds have the potential use in a vast array of research applications including solar cells,[40] sensors,[41] separations, and biomedical.[30, 33, 39] Herein, we present a hyperthermal technique involving NIR laser irradiation to generate photothermal energy from a GUMBOS-based near-infrared compound composed of a cationic dye and biocompatible folate anion. Several NIR active GUMBOS are evaluated to correlate composition with heating efficiency, cell uptake and cytotoxicity.

Experimental

Materials. The following chemicals were purchased from Sigma-Aldrich (St. Louis, MO) without further purification: folic acid, 1-Butyl-2-[2-[3-[(1-butyl-6-chlorobenz[cd]indol-2(1*H*)-ylidene)ethylidene]-2-chloro-1-cyclohexen-1-yl]ethenyl]-6-chlorobenz[cd]indolium tetrafluoroborate ([1048][BF_4]) and 4-[2-[2-Chloro-3-[(2,6-diphenyl-4*H*-thiopyran-4-ylidene)ethylidene]-1-cyclohexen-1-yl]ethenyl]-2,6-diphenylthiopyrylium tetrafluoroborate ([1061][BF_4]), 18.2 MΩ deionized water (DI), sodium hydroxide (NaOH), dichloromethane (DCM), dimethyl sulfoxide (DMSO), acetonitrile, and acetone. AlamarBlue® assay, LIVE/DEAD® Viability/Cytotoxicity Kit (live: calcein-AM and dead: ethidium homodimer-1), and Dulbecco's Modified Eagle Media (DMEM) were purchased from Invitrogen Life Technologies Corporation (Grand Island, NY). The DMEM was modified with 10% Fetal Bovine Serum, 15 mM HEPES, glutamax 100X, non-essential amino acids (NEAA 100X), and sodium pyruvate (NaPyr 100X). Phosphate buffer saline (PBS) was purchased from Fisher Scientific: BioReagents (Fair Lawn, NJ). The malignant MDA-MB-231 and non-malignant HS-578-BST human epithelial breast cells were obtained from ATCC (Manassas, VA) for *in vitro* studies. The cells were cultured in DMEM modified buffer at 37 °C and 5% CO_2.

Characterization Techniques. The GUMBOS and nanoGUMBOS infrared absorption measurements were characterized by a Lambda 750 UV-Vis-NIR Spectrophotometer (Perkin-Elmer, Waltham, MA, USA) using a 1 cm path length quartz cuvet. Structural characterizations of the GUMBOS were elucidated by the following instruments: Agilent 6210 Electrospray Time-of-

Flight Mass Spectrometer, ^{19}F NMR Brüker DPX-250 (250 MHz). Transmission electron microscopy (TEM) images were generated using a JEOL JEM-1011. Dynamic light scattering (DLS) studies were performed with a Zetasizer Nanoseries Nano ZS (Malvern Instruments, Worcestershire, UK) instrument. Fluorescence intensity from the cell assays were recorded from a Wallace Victor2™ (Perkin-Elmer, Waltham, MA, USA) plate reader. Visualizations of the fluorescent live/dead probe were observed by an Olympus IX81 microscope with Hammamatsu C4742 fluorescence detector.

Synthesis of GUMBOS and NanoGUMBOS. Folic acid was converted into sodium folate by 24 hour mixing a 1:1 mol:mol ratio of folic acid and NaOH at ambient conditions. Sodium folate confirmation was supported by electrospray mass spectrometry (ESI MS) (Figure S1). The ESI MS spectrum shows that the folate peak (m/z = 464) was about half of the folic acid peak (m/z = 442), suggesting that only half of the reactant was deprotonated forming sodium folate. The GUMBOS were synthesized via anion exchange method. The NIR absorbing cationic dyes, [1048] and [1061], were individually dissolved in DCM and mixed with the aqueous (2:1 v/v) folate in a 1:2 mol:mol ratio (Scheme 1). The synthesis method uses a 1:2 mol:mol ratio of cation:anion precursors, as approximately half of the folate starting material is sodium folate according to the mass spectrum. The materials were allowed to mix thoroughly and precipitate for two days at ambient conditions wrapped in aluminum foil to avoid photobleaching, prior to washing and purification. The newly synthesized GUMBOS were washed three times and stored in the dark at ambient temperatures. Successful metathesis reactions were supported by ^{19}F NMR (Figure S2).

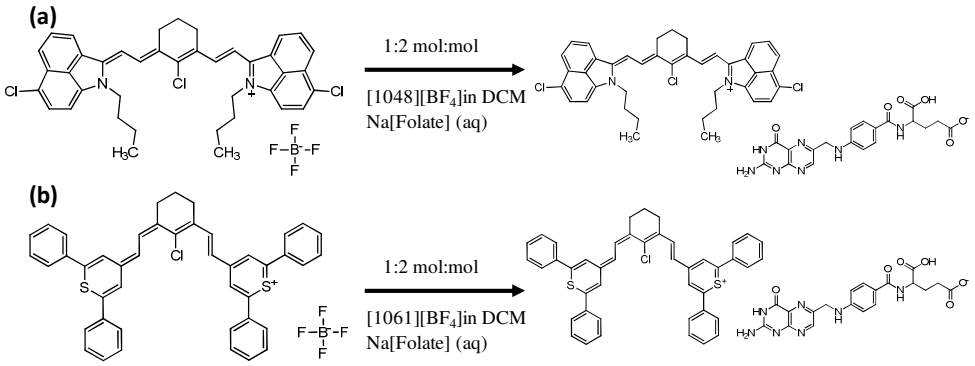

Scheme 1. A metathesis reaction exchanging a folate anion with tetrafluoroborate was done in a 1:2 mol:mol ratio to synthesize (a) [1048][Folate] and (b) [1061][Folate].

NanoGUMBOS were synthesized by a microwave-assisted reprecipitation method in triply distilled 18.2 MΩ water. The GUMBOS were dissolved in acetone at concentration of 2 mM and injected in the DI water accordingly to have final nanoGUMBOS concentration of 320 μg mL^{-1} in 5 mL of an aqueous suspension. The microwave parameters were set to ramp at 3.33 °C s^{-1} up to 150 °C and held for five minutes. The aqueous suspended nanoGUMBOS product was drop-cast on a 400 mesh ultrathin carbon-film copper TEM grid (Ted Pella Inc., Redding, CA, USA) and DLS was measured in triplicate. The wavelength of analysis for measuring insolubility was determined by comparing the absorbance maxima for a well-dispersed nanoGUMBOS concentration (32 μg mL^{-1}) and that same concentration post centrifugation. To determine the dissolution of the nanoGUMBOS

in aqueous solution the particles were suspended in DI water at ambient conditions for two weeks followed by centrifugation for 20 minutes at 3500 rpm before the top-most supernatant was assayed for absorbance (Figure S3). Differences in absorbance pre and post centrifugation were quantified to determine change in soluble concentration. The absorbance was baselined using triply distilled deionized water before each absorption measurement.

Cell Cytotoxicity of NanoGUMBOS. The cytotoxicity of nanoGUMBOS was tested nine times against malignant MDA-MB-231 and non-malignant HS-578-BST epithelial human breast cells. Concentrations of 100 µL of 1x 10^4 of MDA-MB-231 and 5x 10^3 of HS-578-BST cells were seeded in tissue cultured 96 well plate and incubated for 24 hours at 37 °C and 5% CO_2. The media was exchanged with fresh 100 µL of DMEM and different volumes of 320 µg mL^{-1} nanoGUMBOS (4, 16, 32, 64, and 128 µL) were added to cells for an incubation of 24 hours. Once injected, the final nanoGUMBOS concentrations in the well plates were respectively 12.3, 44.1, 77.6, 124.9, and 179.6 µg mL^{-1}. The media was removed, washed with PBS and the cells were incubated with 100 µL of the 10% v/v alamarBlue® in DMEM for four hours. The fluorescence intensity of alamarBlue® (Ex = 530 nm and Em = 620 nm) was measured with a Wallac VICTOR2 V 1420-040 multilabel counter. Live and dead (3% H_2O_2 injection) controls for both cell lines were also administered. The nanoGUMBOS percent viability averages and +/- standard deviations were compared against the fluorescence intensity from the live controls.

NIR Laser Irradiation Control. Laser irradiation source was (1064 nm) from a diode-pumped continuous solid-state Nd:YVO_4 laser (Lasermate Group Inc., Pomona, CA, USA). Cells prepared as previously mentioned underwent variable duration of NIR laser irradiation at 32 W cm^{-2} *sans* nanoGUMBOS as a laser exposure control. The laser exposure control was performed nine times using freshly cultured cells. Cells were irradiated for 10, 20, or 30 minutes followed by immediate removal of the media, then washed with PBS, and incubated in 100 µL of 10% v/v alamarBlue®. Assay plate readings were performed four hours after 100 µL addition of the dye. The laser irradiation percent viability averages and +/- standard deviations were compared against the fluorescence intensity from the live controls.

Hyperthermal Technique. Cells were prepared as previously described above. NanoGUMBOS with final concentrations of 77.6, 124.9, and 179.6 µg mL^{-1} were cultured with MDA-MB-231 and HS-578-BST cells for eight hours before irradiating the wells with a 2 mm beam diameter NIR laser (Figure S4). The hyperthermal irradiation was performed orthogonally with the laser 2.5 cm above the 96 well plate to ensure homogeneity. Each well plate was exposed to continuous NIR laser irradiation for either 10, 20, or 30 minutes with a laser power density of 32 W cm^{-2}. Nine individual samples were performed for each NIR laser irradiation time in a freshly cell-cultured well. After irradiation the media was removed, cells were washed with PBS, and incubated with 100 µL of the 10% v/v alamarBlue® in DMEM for four hours prior to measuring fluorescence. The hyperthermal percent viability averages and +/- standard deviations were compared against the fluorescence intensity from the live controls.

Fluorescence Microscopy. Fluorescence microscopy was used to qualitatively image cell death via hyperthermia by co-labeling the cells with LIVE/DEAD® Viability Kit for mammalian cells. A 1 mL of 2.5 x 10^5 cells mL^{-1} of MDA-MB-231 cell solution

was seeded in a 12 well plate and incubated for 24 – 48 hours until confluent. The cells were cultured with 77.6 μg mL^{-1} nanoGUMBOS and allowed to incubate for eight hours before irradiating the cells for 30 minutes. The cells were stained after irradiation with the LIVE/DEAD® Viability Kit according to manufacturer's instructions.

Photothermal Measurements. The variable concentrations of nanoGUMBOS were subjected to NIR laser irradiation for at least 30 minutes. Incremental volumes (i.e. 0, 32, 64, and 128 μL) of 320 μg mL^{-1} nanoGUMBOS were added to a glass NMR tube filled with 100 μL of DMEM media. The final nanoGUMBOS concentrations were the following, respectively: 0, 77.6, 124.9, and 179.6 μg mL^{-1}. A 2 mm beam diameter of NIR laser irradiation was applied to each sample in triplicates at a power of 32 W cm^{-2}, and measured with a TA (Thermal Analysis) Instruments Thermocouple placed 2 mm above the irradiation spot and Universal Analysis 2000 program (version 4.3A) (Figure S5).

Cellular Uptake. Cellular uptake of nanoGUMBOS was measured employing modified previous methods and performed in triplicate.[42, 43] A concentration of 77.6 μg mL^{-1} NanoGUMBOS solution was incubated with 1 mL of 2.5 x 10^5 mL^{-1} MDA-MB-231 cell solution in a 12 well plate for eight hours. The media was removed and the cells were washed in triplicate with PBS. The washed cells were digested using 2 mL of DMSO. A GUMBOS concentration equivalent to 77.6 μg mL^{-1} was dissolved in DMSO to be a reference against a DMSO-digested cell reference (Figure S7). The absorbance measurements were compared to a concentration gradient of nanoGUMBOS concentrations dissolved in DMSO (Figure S8).

Results and Discussion

Recently, several studies have described the use of gold nanomaterials (e.g. shells, particles, and rods) in producing heat by NIR laser irradiation for hyperthermia.[44-46] The laser wavelengths for NIR irradiation is at a typically shorter wavelengths (800 nm) for nanoparticle hyperthermia from surface plasmon resonance. Herein a new class of materials called NIR absorbing nanoGUMBOS demonstrates photothermal generation for use as a potential hyperthermal cancer therapeutic. A potential advantage of this system, compared to nanoplasmonic NIR hyperthermic systems is the flexibility of composition in that both of the ionic constituents of the GUMBOS system can be varied to provide wide range of achievable spectroscopic, and cytocompatibility properties. The two different NIR absorbing nanoGUMBOS, [1048][Folate] and [1061][Folate], with similar spectroscopic properties were compared in the study. The aforementioned NIR absorbing nanoGUMBOS were selected based on the overlap of absorbance maximum (i.e. 1048 and 1061 nm, respectively) to laser irradiation wavelength and human tissue absorbance minima[22] in order to maximize tissue penetration and delivery of photothermal energy (Figure 1). Folate was selected as a counterion as the over expression of folate receptor in cancer cells provides a well described targeting modality.

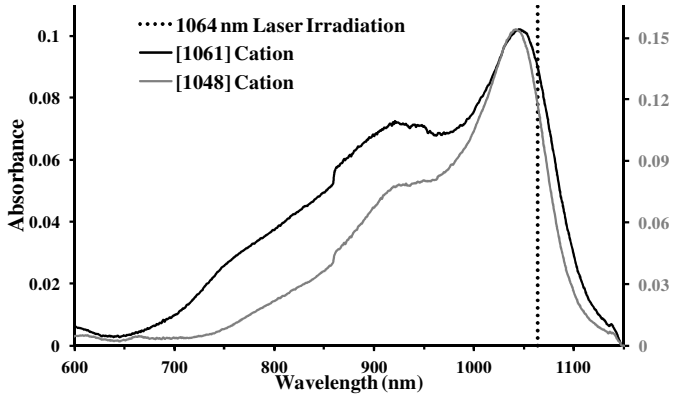

Figure 1. The 4.3 μM GUMBOS dissolved in acetonitrile resulted in absorbance maximum near the laser irradiation wavelength.

NIR Absorbing NanoGUMBOS Characterization. A microwave-assisted reprecipitation method was used to synthesize NIR absorbing nanoGUMBOS from GUMBOS. The TEM micrographs (Figure 2) and DLS (Table 1) for [1048][Folate] and [1061][Folate] NIR absorbing nanoGUMBOS revealed relatively nonaggregating particles. The [1061][Folate] nanoGUMBOS particles resulted in a low polydispersity index (PDI), which supports the TEM micrograph displaying relatively monodisperse particles. The higher PDI for [1048][Folate] nanoGUMBOS is within the acceptable range of dispersity, but as evident in the TEM micrograph there is more aggregation resulting in a higher polydispersity.[47] Nanoparticles are typically reported to have a larger size with DLS, compared to TEM measurements, as the DLS measures the average hydrodynamic radius. The NIR absorbing nanoGUMBOS were determined to be 89 – 93% insoluble after a two week study of the particles suspended in water (Table 2). It is worthy of noting that a red-shift in nanoGUMBOS absorbance maximum occurred with respect to the dissolved counterpart.[37, 48, 49]

Table 1. The NIR nanoGUMBOS were monodisperse under microwave-assisted reprecipitation synthesis.

NanoGUMBOS	NanoGUMBOS size (nm)		
	TEM Micrograph	DLS	PDI
[1048][Folate]	121 ± 32.5	157 ± 2.4	0.137
[1061][Folate]	144 ± 46.8	176 ± 1.2	0.066

Table 2. NIR nanoGUMBOS remained largely insoluble in an aqueous suspension media for two weeks when compared to a standard curve from the appropriate concentration gradient.

NanoGUMBOS	Wavelength (nm) Maximum	Absorbance		% Difference	% Insoluble
		Control	Centrifuged		
[1048][Folate]	1077	0.219123	0.015503	7.08	92.92
[1061][Folate]	1118	0.051012	0.005738	11.25	88.75

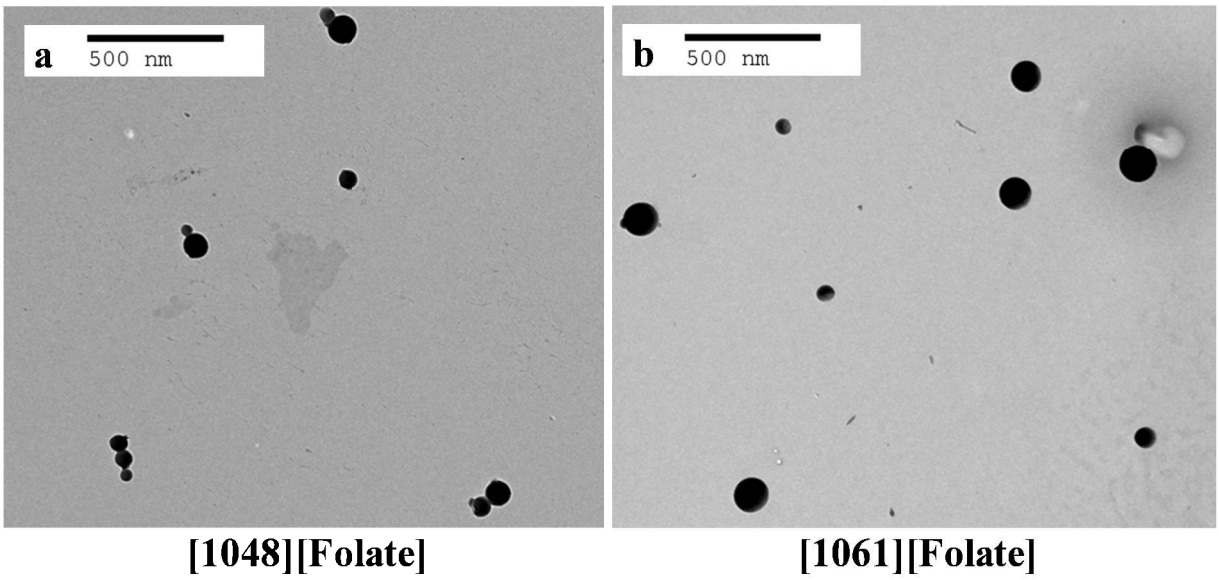

Figure 2. The NIR absorbing nanoGUMBOS TEM micrograph shows particle sizes for (a) [1048][Folate] at 121 ± 32.5 nm and (b) [1061][Folate] at 144 ± 46.8 nm.

NIR Absorbing NanoGUMBOS Cytotoxicity. NIR Absorbing nanoGUMBOS cytotoxicity was determined in a cancerous breast cell line (MDA-MB-231) and non-malignant breast cell line (HS-578-BST) by an alamarBlue® assay (Figure 3) from nine individual samples.[50, 51] The NIR absorbing nanoGUMBOS were toxic to both cell lines at high concentration; however, the nanoGUMBOS were more toxic to MDA-MB-231 cells, likely as a result of increased folate receptor alpha (FRA) expression in the malignant cell membrane (Table S1). The median lethal concentration (LC_{50}) of NIR absorbing nanoGUMBOS was calculated from the slope at which the cell viability decreased (Figure S6). The LC_{50} for NIR absorbing nanoGUMBOS [1048][Folate] in MDA-MB-231 and HS-578-BST cell lines are 158 and 225 μg mL^{-1}, respectively. The [1061][Folate] nanoGUMBOS LC_{50} for MDA-MB-231 and HS-578-BST are 118 and 348 μg mL^{-1}, respectively. The increase in [1061][Folate] toxicity at high concentration, when compared to [1048][Folate], remains unexplained and requires further analysis.

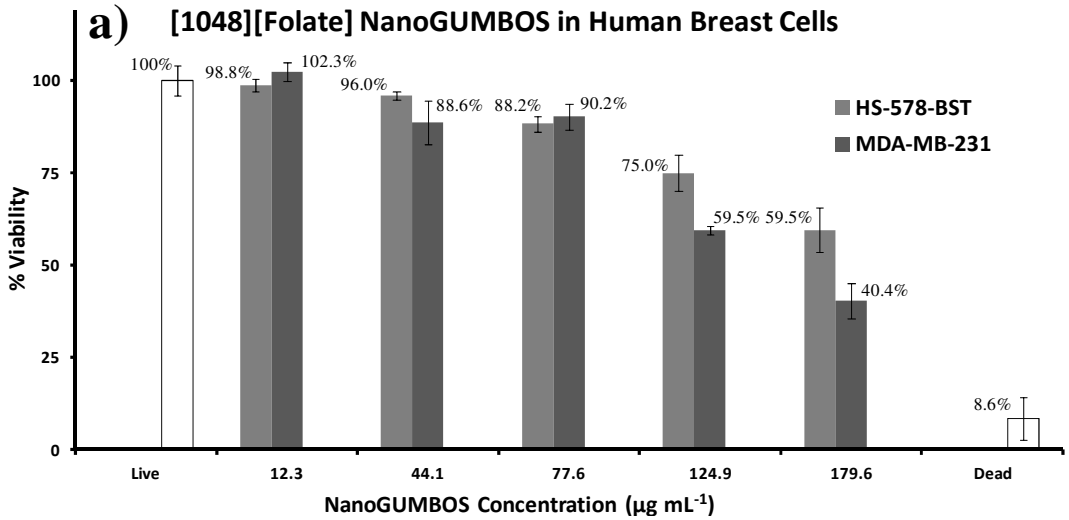

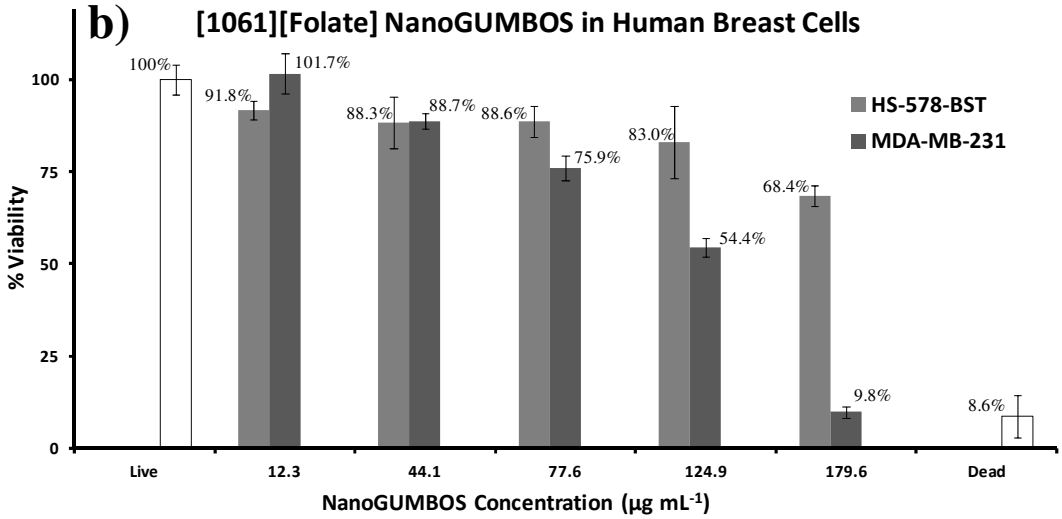

Figure 3. Viability studies of (a) [1048][Folate] and (b) [1061][Folate] NIR absorbing nanoGUMBOS using an alamarBlue® assay was performed on breast cell lines. The viability averages were calculated from the mean of nine individual samples for each concentration, and the respective +/- standard deviations are given in the supplementary information.

Laser Irradiation Cytotoxicity. Since the late 19th century, it has been known that healthy cells are more tolerant of elevated temperature than cancer cells by providing a simple means for selectively attacking cancer cells in a heterogeneous population.[52, 53] Irradiation of cells was performed orthogonally to a 96 well plate over a defined period from 0-30 minutes. In the irradiation control, normal breast cells retained 93 – 96% viability after continuous irradiation, whereas the viability of the cancerous cells decreased (Figure 4). Cancer cells are more susceptible to heat due to disorganized cellular structure and functions.

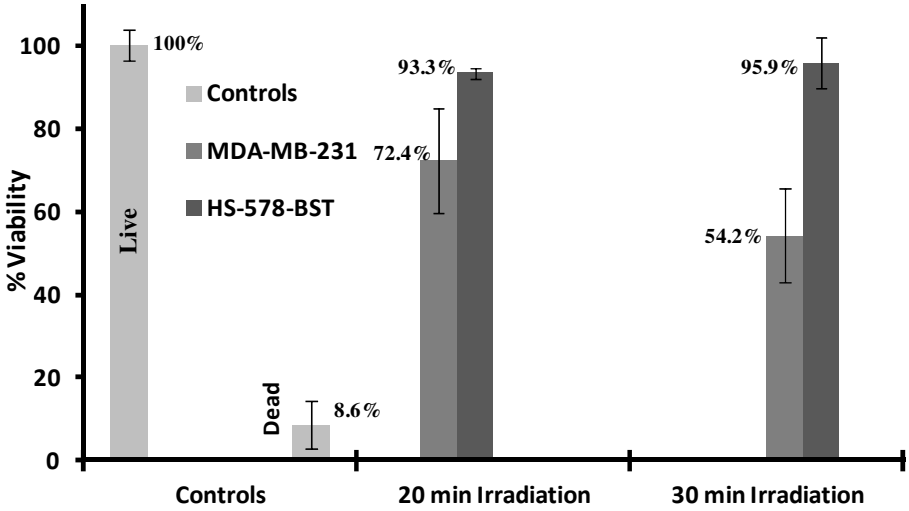

Figure 4. Laser irradiation without an injection of nanoGUMBOS over cancerous MDA-MB-231 and noncancerous HS-578-BST were observed. The viability averages were calculated from the mean of nine individual samples for each irradiation time length, and the respective +/- standard deviations are given in the supplementary information.

Hyperthermia Testing with Cancer Cells. When the MDA-MB-231 cells with NIR absorbing nanoGUMBOS were irradiated, it was concluded that the 77.6 μg mL^{-1} concentration under irradiation for 20 minutes resulted in a reduction in tumor cell viability for both nanoGUMBOS compared to particle only controls. A side-by-side comparison of [1048][Folate] (Figure 5) and [1061][Folate] (Figure 6) nanoGUMBOS cytotoxicity, hyperthermia responses, and laser control toxicity with MDA-MB-231 cancer cells demonstrates the effectiveness of the nanoGUMBOS.

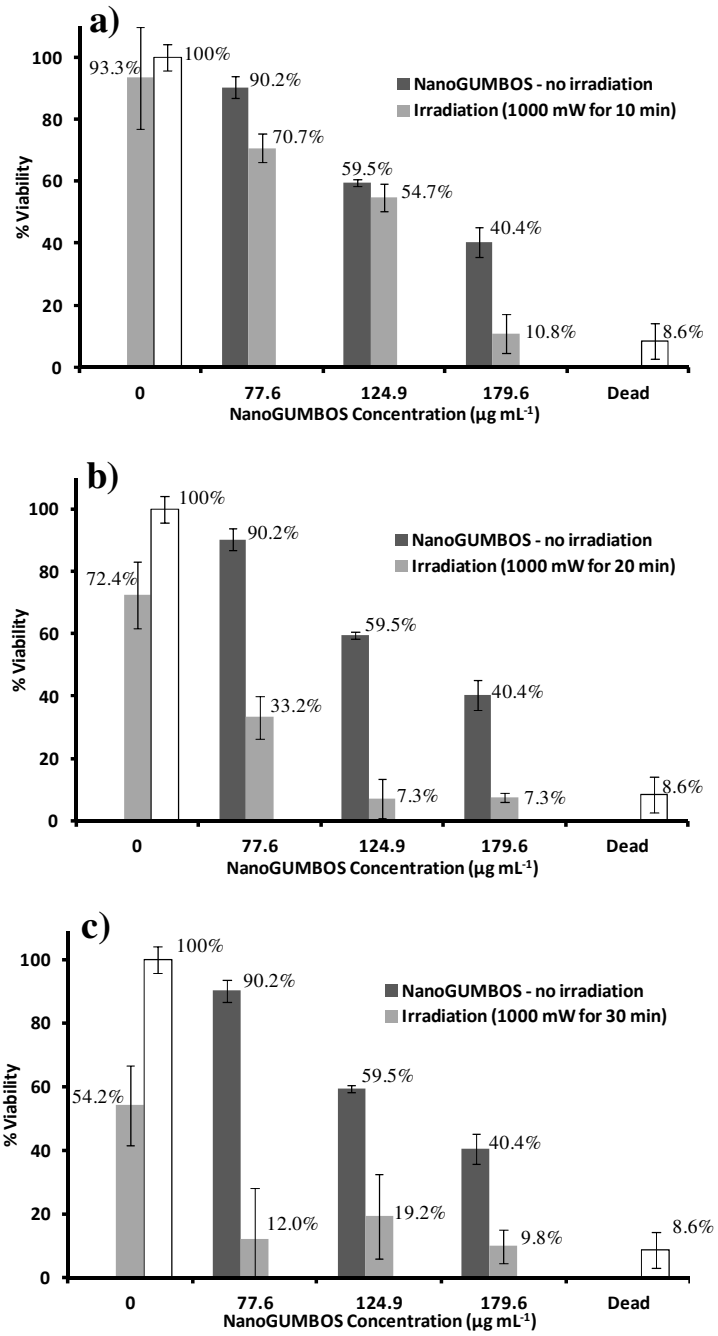

Figure 5. [1048][Folate] NIR nanoGUMBOS with MDA-MB-231 breast cancer cells shows live and dead controls (white), nanoGUMBOS cytotoxicity-dark gray, and hyperthermal (laser and nanoGUMBOS)-light gray at (a) 10 minute, (b) 20 minute,

and (c) 30 minute lasing time intervals. The viability averages were calculated from the mean of nine individual samples for each test, and the respective +/- standard deviations are given in the supplementary information.

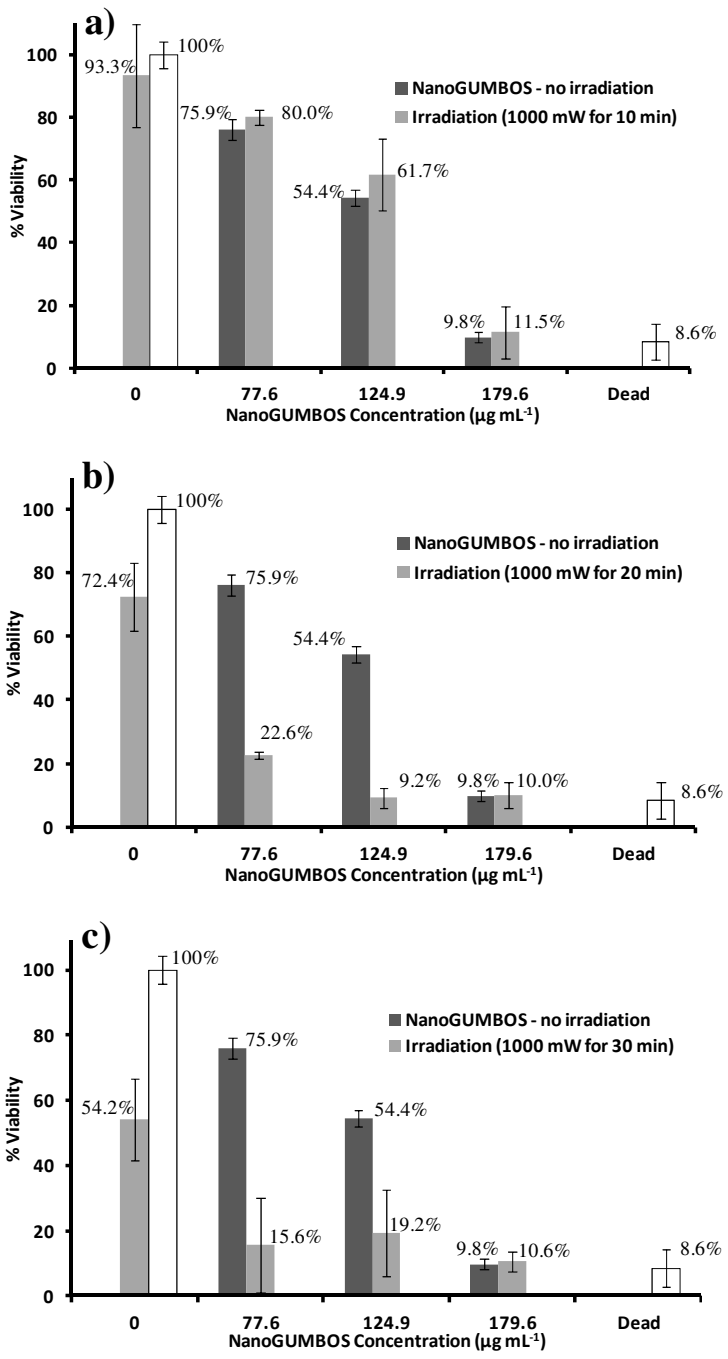

Figure 6. [1061][Folate] NIR nanoGUMBOS with MDA-MB-231 breast cancer cells shows live and dead controls (white), nanoGUMBOS cytotoxicity-dark gray, and hyperthermal (laser and nanoGUMBOS)-light gray at (a) 10 minute, (b) 20 minute, and (c) 30 minute lasing time intervals. The viability averages were calculated from the mean of nine individual samples for each test, and the respective +/- standard deviations are given in the supplementary information.

The application of [1048][Folate] nanoGUMBOS in concert with NIR laser irradiation resulted in substantial reductions in viable cancer cells at the lowest nanoGUMBOS concentration and exposure times. It was also shown that with an increase in irradiation time and nanoGUMBOS concentration the lethality of the nanoGUMBOS increased (Table S2). The concentration of 77.6 μg mL^{-1} and 10, 20, and 30 minutes irradiation resulted in respective cell viability average percentages of 70.7, 33.2, and 12.0%. This concentration would be optimal as the nanoGUMBOS control yielded a mean cell viability of 90.2%.

The [1061][Folate] nanoGUMBOS in concert with NIR laser irradiation also substantially reduced cancer cells viability at concentration of 77.6 μg mL^{-1}. This concentration with 10, 20, and 30 minute irradiation resulted in respective cell viability averages of 80.0, 22.6, and 15.6%. After 10 minutes of irradiation, the nanoGUMBOS control and nanoGUMBOS with irradiation resulted in similar cell death indicating little contribution of the photothermal effects. The reduced efficacy of the irradiated [1061][Folate] nanoGUMBOS at the 10 minute time point can potentially be attributed to a reduced cellular uptake or reduced nanoGUMBOS stability in aqueous solution. Alternatively, the difference in activity for [1061][Folate] and [1048][Folate] nanoGUMBOS at the 10 minute time point may indicate a more complex cytotoxic mechanism such as a combination of hyperthermal and singlet oxygen production. Nonetheless, at 20 and 30 minute irradiation, there were similar differences between the particle control and irradiated group demonstrating hyperthermal activity. The two irradiation times did not exhibit a noticeable difference in cell death outside standard deviations but it can be theorized that longer irradiation times would increase cell death. At high concentration the nanoGUMBOS were equally toxic with or without irradiation. This is predictable as this concentration is approximately the LC_{50} threshold for [1061][Folate] (Figure 3b).

The fluorescence microscopy image qualitatively shows the spatial selectivity of cell death when a NIR laser irradiates nanoGUMBOS (i.e. 77.6 μg mL^{-1} [1048][Folate]) treated cancerous breast cells for 30 minutes (Figure 7). The cells have been assayed using a LIVE/DEAD® fluorescent staining kit, which stains live and dead cells, green and red respectively. Cells in the light exposed region have either exhibited ablation (Figure 7a, no fluorescence) or died (Figure 7b, indicated by red fluorescence). Cells outside the laser spot region (Figure 7c, green fluorescence) are clearly green indicating continued viability post-exposure.

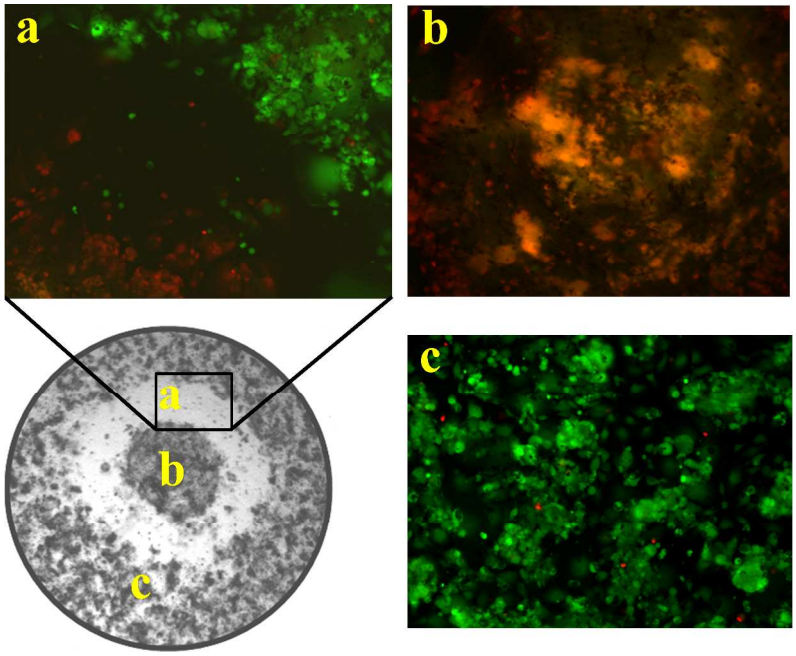

Figure 7. A fluorescence microscopy image from a well plate with breast cancer cells distinctively shows cell death from the selective area where (a) the cusp of irradiation/nonirradiation occurred as shown in the inset, (b) laser irradiation occurred, and (c) did not occur. (Note: the diameter of the laser spot matches the laser focal spot in image, 2 mm.)

Laser Irradiation Photothermal Response. The NIR absorbing nanoGUMBOS generated heat from the radiationless vibrational relaxations after excitation to the first excited singlet state. Recording hyperthermal generation proved difficult in a 96 well plate due to the laser irradiating the thermocouple directly. In an effort to accurately record the photothermal generation of the nanoGUMBOS, a glass NMR tube was used as the test cell to mimic the conditions cells would experience in a 96 well plate. Also, using a thermocouple increases temperature data reliability by reducing the Newton's law of cooling (including: radiative, evaporative, and connective cooling) factor that thermal imaging cameras encounter.[54] In this configuration the thermocouple could be submerged in the test media but out of the direct path of the NIR laser. The NIR absorbing nanoGUMBOS were irradiated in 100 µL modified DMEM media for 30 minutes while the thermocouple measured photothermal generation (Figure 8). The experiment is designed to determine the maximum photothermal temperature generated and temperature dependence as a function of irradiation time.[20, 55] NanoGUMBOS concentrations for laser irradiation were the same as used in the concentration dependent viability experiments: 77.6, 124.9, and 179.6 µg mL^{-1} (Table S3).

All of the [1048][Folate] NIR absorbing nanoGUMBOS reached a photothermal steady state after 10 minutes of continuous irradiation. After 30 minutes of irradiation [1048][Folate] NIR absorbing nanoGUMBOS concentrations of 77.6, 124.9, and 179.6 µg mL^{-1} respectively heated to 48.1 ± 4.2, 59.9 ± 1.9, and 57.5 ± 6.2 °C. The [1061][Folate] NIR absorbing nanoGUMBOS achieved steady state more rapidly, stabilizing after five minutes. The [1061][Folate] NIR absorbing nanoGUMBOS of

concentrations 77.6, 124.9, and 179.6 μg mL^{-1} respectively heated to 55.4 ± 4.0, 63.2 ± 2.4, 64.3 ± 2.2 °C. The higher steady state temperature achieved by the [1061][Folate] is likely a result of larger sized particles ($\bar{x}$ = 144 ± 46.8 nm) relative to [1048][Folate] ($\bar{x}$ = 121 ± 32.5 nm). The increased photothermal generation correlated with an increase in cytotoxicity for [1048][Folate] and [1061][Folate] nanoGUMBOS. In addition to hyperthermia cytotoxicity, other factors such as oxygen radical formation may have contributed to overall cell death which can be explored further.[56, 57] The experimental error for [1048][Folate] reveals that the difference in photothermal generation between the media control and the lowest concentration of nanoGUMBOS (77.6 μg mL^{-1}) is slight; but at higher concentrations the temperature differential is larger. Concentrations for the [1061][Folate] samples had a large disparity in temperature differences relative from the DMEM media control.

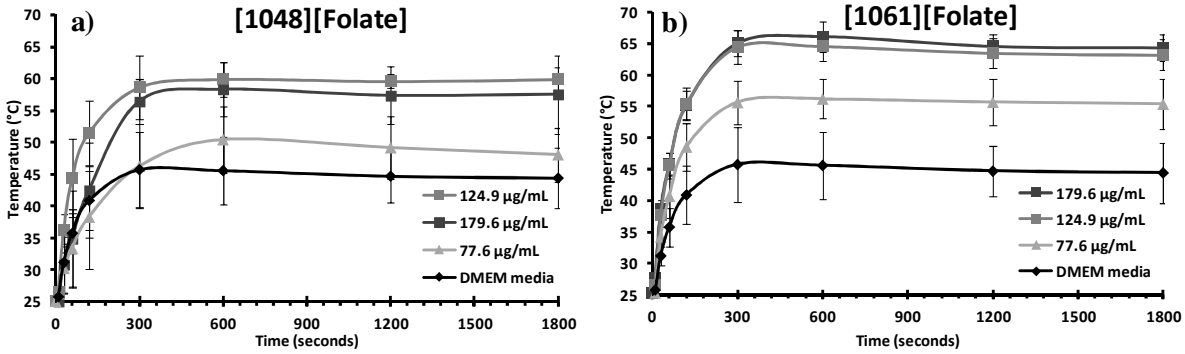

Figure 8. Heat generated from the NIR absorbing nanoGUMBOS (a) [1048][Folate] and (b) [1061][Folate]. The photothermal temperature averages were calculated from the mean of triplicate samples for each concentration, and the respective +/- standard deviations are given in the supplementary information.

Cellular Uptake of NanoGUMBOS in MDA-MB-231. Receptor-mediated endocytosis is initiated by cell surface receptor interactions initiating a cascade which results in cell wall invagination and nanomaterial uptake.[26, 27, 58] After performing the method (*vide supra*) for cellular uptake it was determined that only about 6% of the injected (77.6 μg mL^{-1}) entered the MDA-MB-231 cells (Table 3). Confirmation of the cellular uptake was performed by calculating percent yield from the absorbencies differences (% Yield Uptake) and from a nanoGUMBOS concentration gradient (% Slope). The 1000 nm wavelength was chosen as an absorbance point as there did not seem to be any substantial changes in spectral shift or characteristic between the two samples. The 77.6 μg mL^{-1} nanoGUMBOS were dissolved in DMSO and subsequently diluted to create a concentration gradient (Figure S8). The smaller particle size for [1048][Folate] may account for the slightly higher overall cellular uptake.

Table 3. The percent of nanoGUMBOS in MDA-MB-231 cells were calculated from the percent yield and concentration gradient equation (%Slope).

NanoGUMBOS	Sample	Wavelength (nm)	Absorbance	%Yield Uptake	%Slope
[1048][Folate]	**Cells**	1000	0.004986	6.34	6.15
	Reference		0.078640		

[1061][Folate]	**Cells** / **Reference**	1000	0.002146 / 0.038080	5.64	6.12

Conclusion

The [1048][Folate] and [1061][Folate] NIR absorbing nanoGUMBOS both reduced the viability of MDA-MB-231 breast cancer cells when activated by 1064 nm NIR laser irradiation. NIR absorbing nanoGUMBOS without irradiation showed little cytotoxicity to both cancerous (MDA-MB-231) and non-cancerous (HS-578-BST) breast cells at low concentrations. While [1061][Folate] produced a greater steady state temperature when irradiated, this did not correlate with a greater cytotoxicity; however both irradiated nanoGUMBOS reduced viable MDA-MB-231 cells compared to non-irradiated controls. The integrity of both nanoGUMBOS composition remained consistent neither having substantial particle degradation nor change in solubility after two weeks in an aqueous media. Based on these results, this class of folate-based NIR absorbing nanoGUMBOS has demonstrated potential applicability as an alternative hyperthermal delivery system.

Acknowledgements

The authors would like to thank the National Science Foundation (NSF 0911118) for funding this research.

Notes and references

[a]Department of Chemistry and [b]Department of Biological and Agricultural Engineering, Louisiana State University, Baton Rouge, LA 70803, USA

Present Address

[§]Current address: Department of Mechanical and Materials Engineering, Florida International University, Miami, FL 33174, USA

Supporting Information

†Electronic Supplementary Information (ESI) available: ESI MS, ^{19}F NMR, absorbance spectrum for solubility and cellular uptake, cytotoxicity and photothermia tables, and LC_{50} graph for the nanoGUMBOS is available free of charge. See DOI: 10.1039/b000000x/

References

1. American Cancer Society. Cancer Facts & Figures 2014. http://www.cancer.org/acs/groups/content/@research/documents/document/acspc-041780.pdf (accessed May 26, 2014).
2. D. A. Berry, K. A. Cronin, S. K. Plevritis, D. G. Fryback, L. Clarke, M. Zelen, J. S. Mandelblatt, A. Y. Yakovlev, J. D. F. Habbema, E. J. Feuer and C. Collaborators, Effect of Screening and Adjuvant Therapy on Mortality from Breast Cancer, *N. Engl. J. Med.*, 2005, **353**, 1784-1792.
3. E. S. Glazer and S. A. Curley, The Ongoing History of Thermal Therapy for Cancer, *Surg. Oncol. Clin. N. Am.*, 2011, **20**, 229-235.
4. R. Kitture, S. Ghosh, P. Kulkarni, X. L. Liu, D. Maity, S. I. Patil, D. Jun, Y. Dushing, S. L. Laware, B. A. Chopade and S. N. Kale, Fe_3O_4-Citrate-Curcumin: Promising Conjugates for Superoxide Scavenging, Tumor Suppression and Cancer Hyperthermia, *J. Appl. Phys.*, 2012, **111**, 064702.
5. D. K. Kim, M. S. Amin, S. Elborai, S. H. Lee, Y. Koseoglu and M. Muhammed, Energy Absorption of Superparamagnetic Iron Oxide Nanoparticles by Microwave Irradiation, *J. Appl. Phys.*, 2005, **97**, 10J510.

6. Z. Fan, D. Senapati, S. A. Khan, A. K. Singh, A. Hamme, B. Yust, D. Sardar and P. C. Ray, Popcorn-Shaped Magnetic CorePlasmonic Shell Multifunctional Nanoparticles for the Targeted Magnetic Separation and Enrichment, Label-Free SERS Imaging, and Photothermal Destruction of Multidrug-Resistant Bacteria, *Chem.-Eur. J.*, 2013, **19**, 2839-2847.
7. K. E. Peyer, S. Tottori, F. M. Qiu, L. Zhang and B. J. Nelson, Magnetic Helical Micromachines, *Chem.-Eur. J.*, 2013, **19**, 28-38.
8. K. H. Bae, M. Park, M. J. Do, N. Lee, J. H. Ryu, G. W. Kim, C. Kim, T. G. Park and T. Hyeon, Chitosan Oligosaccharide-Stabilized Ferrimagnetic Iron Oxide Nanocubes for Magnetically Modulated Cancer Hyperthermia, *ACS Nano*, 2012, **6**, 5266-5273.
9. F. P. Gao, Y. Y. Cai, J. Zhou, X. X. Xie, W. W. Ouyang, Y. H. Zhang, X. F. Wang, X. D. Zhang, X. W. Wang, L. Y. Zhao and J. T. Tang, Pullulan Acetate Coated Magnetite Nanoparticles for Hyper-Thermia: Preparation, Characterization and In Vitro Experiments, *Nano Res.*, 2010, **3**, 23-31.
10. D.-H. Kim, E. A. Vitol, J. Liu, S. Balasubramanian, D. J. Gosztola, E. E. Cohen, V. Novosad and E. A. Rozhkova, Stimuli-Responsive Magnetic Nanomicelles as Multifunctional Heat and Cargo Delivery Vehicles, *Langmuir: the ACS journal of surfaces and colloids*, 2013, **29**, 7425-7432.
11. J. Li, J. Han, T. Xu, C. Guo, X. Bu, H. Zhang, L. Wang, H. Sun and B. Yang, Coating Urchinlike Gold Nanoparticles with Polypyrrole Thin Shells to Produce Photothermal Agents with High Stability and Photothermal Transduction Efficiency, *Langmuir : the ACS journal of surfaces and colloids*, 2013, **29**, 7102-7110.
12. Y. Y. Su, X. P. Wei, F. Peng, Y. L. Zhong, Y. M. Lu, S. Su, T. T. Xu, S. T. Lee and Y. He, Gold Nanoparticles-Decorated Silicon Nanowires as Highly Efficient Near-Infrared Hyperthermia Agents for Cancer Cells Destruction, *Nano Letters*, 2012, **12**, 1845-1850.
13. J. T. Robinson, K. Welsher, S. M. Tabakman, S. P. Sherlock, H. L. Wang, R. Luong and H. J. Dai, High Performance In Vivo Near-IR (> 1 μm) Imaging and Photothermal Cancer Therapy with Carbon Nanotubes, *Nano Res.*, 2010, **3**, 779-793.
14. X. H. Huang, I. H. El-Sayed, W. Qian and M. A. El-Sayed, Cancer Cell Imaging and Photothermal Therapy in the Near-Infrared Region by Using Gold Nanorods, *J. Am. Chem. Soc.*, 2006, **128**, 2115-2120.
15. L. R. Hirsch, R. J. Stafford, J. A. Bankson, S. R. Sershen, B. Rivera, R. E. Price, J. D. Hazle, N. J. Halas and J. L. West, Nanoshell-Mediated Near-Infrared Thermal Therapy of Tumors Under Magnetic Resonance Guidance, *Proc. Natl. Acad. Sci. U. S. A.*, 2003, **100**, 13549-13554.
16. L. J. Meng, L. Y. Niu, L. Li, Q. H. Lu, Z. F. Fei and P. J. Dyson, Gold Nanoparticles Grown on Ionic Liquid-Functionalized Single-Walled Carbon Nanotubes: New Materials for Photothermal Therapy, *Chem.-Eur. J.*, 2012, **18**, 13314-13319.
17. P. Yang, Q. Z. Xu, S. Y. Jin, Y. Lu, Y. Zhao and S. H. Yu, Synthesis of Multifunctional Ag@Au@Phenol Formaldehyde Resin Particles Loaded with Folic Acids for Photothermal Therapy, *Chem.-Eur. J.*, 2012, **18**, 9294-9299.
18. B. Pelaz, V. Grazu, A. Ibarra, C. Magen, P. del Pino and J. M. de la Fuente, Tailoring the Synthesis and Heating Ability of Gold Nanoprisms for Bioapplications, *Langmuir*, 2012, **28**, 8965-8970.
19. J. F. Lovell, C. S. Jin, E. Huynh, H. L. Jin, C. Kim, J. L. Rubinstein, W. C. W. Chan, W. G. Cao, L. V. Wang and G. Zheng, Porphysome Nanovesicles Generated by Porphyrin Bilayers for Use as Multimodal Biophotonic Contrast Agents, *Nat. Mater.*, 2011, **10**, 324-332.
20. S. Lal, S. E. Clare and N. J. Halas, Nanoshell-Enabled Photothermal Cancer Therapy: Impending Clinical Impact, *Acc. Chem. Res.*, 2008, **41**, 1842-1851.
21. H. W. Huang and C. T. Liauh, Review: Therapeutical Applications of Heat in Cancer Therapy, *J. Med. Biol. Eng.*, 2012, **32**, 1-10.
22. A. N. Bashkatov, E. A. Genina, V. I. Kochubey and V. V. Tuchin, Optical Properties of Human Skin, Subcutaneous and Mucous Tissues in the Wavelength Range from 400 to 2000 nm, *J. Phys. D: Appl. Phys.*, 2005, **38**, 2543-2555.
23. X. S. Li, G. L. Ferrel, M. C. Guerra, T. Hode, J. A. Lunn, O. Adalsteinsson, R. E. Nordquist, H. Liu and W. R. Chen, Preliminary Safety and Efficacy Results of Laser Immunotherapy for the Treatment of Metastatic Breast Cancer Patients, *Photochem. Photobiol. Sci.*, 2011, **10**, 817-821.
24. B. Sivakumar, R. G. Aswathy, Y. Nagaoka, M. Suzuki, T. Fukuda, Y. Yoshida, T. Maekawa and D. N. Sakthikumar, Multifunctional Carboxymethyl Cellulose-Based Magnetic Nanovector as a Theragnostic System for Folate Receptor Targeted Chemotherapy, Imaging, and Hyperthermia against Cancer, *Langmuir*, 2013, **29**, 3453-3466.
25. D. Bhattacharya, M. Das, D. Mishra, I. Banerjee, S. K. Sahu, T. K. Maiti and P. Pramanik, Folate Receptor Targeted, Carboxymethyl Chitosan Functionalized Iron Oxide Nanoparticles: A Novel Ultradispersed Nanoconjugates for Bimodal Imaging, *Nanoscale*, 2011, **3**, 1653-1662.
26. G. M. van Dam, G. Themelis, L. M. A. Crane, N. J. Harlaar, R. G. Pleijhuis, W. Kelder, A. Sarantopoulos, J. S. de Jong, H. J. G. Arts, A. G. J. van der Zee, J. Bart, P. S. Low and V. Ntziachristos, Intraoperative Tumor-Specific

Fluorescence Imaging in Ovarian Cancer by Folate Receptor-Alpha Targeting: First In-Human Results, *Nat. Med.*, 2011, **17**, 1315-U1202.

27. J. E. Rosen, L. Chan, D. B. Shieh and F. X. Gu, Iron Oxide Nanoparticles for Targeted Cancer Imaging and Diagnostics, *Nanomed. Nanotechnol. Biol. Med.*, 2012, **8**, 275-290.
28. M. Liong, J. Lu, M. Kovochich, T. Xia, S. G. Ruehm, A. E. Nel, F. Tamanoi and J. I. Zink, Multifunctional Inorganic Nanoparticles for Imaging, Targeting, and Drug Delivery, *ACS Nano*, 2008, **2**, 889-896.
29. K. Kaaki, K. Herve-Aubert, M. Chiper, A. Shkilnyy, M. Souce, R. Benoit, A. Paillard, P. Dubois, M. L. Saboungi and I. Chourpa, Magnetic Nanocarriers of Doxorubicin Coated with Poly(ethylene glycol) and Folic Acid: Relation between Coating Structure, Surface Properties, Colloidal Stability, and Cancer Cell Targeting, *Langmuir*, 2012, **28**, 1496-1505.
30. D. K. Bwambok, B. El-Zahab, S. K. Challa, M. Li, L. Chandler, G. A. Baker and I. M. Warner, Near-Infrared Fluorescent NanoGUMBOS for Biomedical Imaging, *ACS Nano*, 2009, **3**, 3854-3860.
31. S. L. de Rooy, B. El-Zahab, M. Li, S. Das, E. Broering, L. Chandler and I. M. Warner, Fluorescent One-Dimensional Nanostructures from a Group of Uniform Materials Based on Organic Salts, *Chem. Commun.*, 2011, **47**, 8916-8918.
32. D. K. Bwambok, S. K. Challa, M. Lowry and I. M. Warner, Amino Acid-Based Fluorescent Chiral Ionic Liquid for Enantiomeric Recognition, *Anal. Chem.*, 2010, **82**, 5028-5037.
33. M. Li, G. M. Ganea, C. F. Lu, S. L. De Rooy, B. El-Zahab, V. E. Fernand, R. Y. Jin, S. Aggarwal and I. M. Warner, Lipophilic Phosphonium-Lanthanide Compounds with Magnetic, Luminescent, and Tumor Targeting Properties, *J. Inorg. Biochem.*, 2012, **107**, 40-46.
34. A. Tesfai, B. El-Zahab, A. T. Kelley, M. Li, J. C. Garno, G. A. Baker and I. M. Warner, Magnetic and Nonmagnetic Nanoparticles from a Group of Uniform Materials Based on Organic Salts, *ACS Nano*, 2009, **3**, 3244-3250.
35. M. Li, S. L. De Rooy, D. K. Bwambok, B. El-Zahab, J. F. DiTusa and I. M. Warner, Magnetic Chiral Ionic Liquids Derived from Amino Acids, *Chem. Commun.*, 2009, **45**, 6922-6924.
36. S. L. de Rooy, M. Li, D. K. Bwambok, B. El-Zahab, S. Challa and I. M. Warner, Ephedrinium-Based Protic Chiral Ionic Liquids for Enantiomeric Recognition, *Chirality*, 2011, **23**, 54-62.
37. J. C. Dumke, A. Qureshi, A. Hamdan, B. El-Zahab, S. Das, D. J. Hayes, D. Boldor, K. Rupnik and I. M. Warner, Photothermal Response of Near-Infrared Absorbing NanoGUMBOS, *Appl. Spectrosc.*, 2014, **68**, 340-352.
38. P. K. S. Magut, S. Das, V. E. Fernand, J. Losso, K. McDonough, B. M. Naylor, S. Aggarwal and I. M. Warner, Tunable Cytotoxicity of Rhodamine 6G via Anion Variations, *J. Am. Chem. Soc.*, 2013, **135**, 15873-15879.
39. M. R. Cole, M. Li, B. El-Zahab, M. E. Janes, D. Hayes and I. M. Warner, Design, Synthesis, and Biological Evaluation of beta-Lactam Antibiotic-Based Imidazolium- and Pyridinium-Type Ionic Liquids, *Chem. Biol. Drug Des.*, 2011, **78**, 33-41.
40. A. N. Jordan, S. Das, N. Siraj, S. L. de Rooy, M. Li, B. El-Zahab, L. Chandler, G. A. Baker and I. M. Warner, Anion-Controlled Morphologies and Spectral Features of Cyanine-Based NanoGUMBOS - An Improved Photosensitizer, *Nanoscale*, 2012, **4**, 5031-5038.
41. B. P. Regmi, J. Monk, B. El-Zahab, S. Das, F. R. Hung, D. J. Hayes and I. M. Warner, A Novel Composite Film for Detection and Molecular Weight Determination of Organic Vapors, *J. Mater. Chem.*, 2012, **22**, 13732-13741.
42. A. Kumar, H. L. Ma, X. Zhang, K. Y. Huang, S. B. Jin, J. Liu, T. Wei, W. P. Cao, G. Z. Zou and X. J. Liang, Gold Nanoparticles Functionalized with Therapeutic and Targeted Peptides for Cancer Treatment, *Biomaterials*, 2012, **33**, 1180-1189.
43. M. K. K. Oo, Y. M. Yang, Y. Hu, M. Gomez, H. Du and H. J. Wang, Gold Nanoparticle-Enhanced and Size-Dependent Generation of Reactive Oxygen Species from Protoporphyrin IX, *ACS Nano*, 2012, **6**, 1939-1947.
44. L. C. Kennedy, L. R. Bickford, N. A. Lewinski, A. J. Coughlin, Y. Hu, E. S. Day, J. L. West and R. A. Drezek, A New Era for Cancer Treatment: Gold-Nanoparticle-Mediated Thermal Therapies, 2011, **7**, 169-183.
45. B. N. Khlebtsov, E. V. Panfilova, G. S. Terentyuk, I. L. Maksimova, A. V. Ivanov and N. G. Khlebtsov, Plasmonic Nanopowders for Photothermal Therapy of Tumors, *Langmuir*, 2012, **28**, 8994-9002.
46. H. Y. Liu, T. L. Liu, X. L. Wu, L. L. Li, L. F. Tan, D. Chen and F. Q. Tang, Targeting Gold Nanoshells on Silica Nanorattles: a Drug Cocktail to Fight Breast Tumors via a Single Irradiation with Near-Infrared Laser Light, *Adv. Mater.*, 2012, **24**, 755-761.
47. P. Russo, A Practical Minicourse in Dynamic Light Scattering. http://msg.lsu.edu/howto/DLS_Minicourse/DLS_Minicourse.pdf (accessed Oct 20, 2013).
48. X. D. Xu and M. B. Cortie, Shape Change and Color Gamut in Gold Nanorods, Dumbbells, and Dog Bones, *Adv. Funct. Mater.*, 2006, **16**, 2170-2176.
49. D. B. Xiao, X. Lu, W. S. Yang, H. B. Fu, Z. G. Shuai, Y. Fang and J. N. Yao, Size-Tunable Emission from 1,3-Diphenyl-5-(2-anthryl)-2-pyrazoline Nanoparticles, *J. Am. Chem. Soc.*, 2003, **125**, 6740-6745.

50. R. S. Huang, S. W. Duan, W. K. Bleibel, E. O. Kistner, W. Zhang, T. A. Clark, T. X. Chen, A. C. Schweitzer, J. E. Blume, N. J. Cox and M. E. Dolan, A Genome-Wide Approach to Identify Genetic Variants that Contribute to Etoposide-Induced Cytotoxicity, *Proc. Natl. Acad. Sci. U. S. A.*, 2007, **104**, 9758-9763.
51. I. M. Tynga, N. N. Houreld and H. Abrahamse, The Primary Subcellular Localization of Zinc Phthalocyanine and its Cellular Impact on Viability, Proliferation and Structure of Breast Cancer Cells (MCF-7), *J. Photochem. Photobiol. B-Biol.*, 2013, **120**, 171-176.
52. J. Byrne, A Digest of 20 Years' Experience in the Treatment of Cancer of the Uterus by Galvanocautery, *Am. J. Obstet. Gynecol.*, 1899, **22**, 1052.
53. L. Loeb, Further Investigations in Transplantation of Tumors, *J. Med. Res.*, 1902, **8**, 44-73.
54. H. C. Huang, K. Rege and J. J. Heys, Spatiotemporal Temperature Distribution and Cancer Cell Death in Response to Extracellular Hyperthermia Induced by Gold Nanorods, *ACS Nano*, 2010, **4**, 2892-2900.
55. J. F. Zhou, L. J. Meng and Q. H. Lu, Core@Shell Nanostructures for Photothermal Conversion: Tunable Noble Metal Nanoshells on Cross-Linked Polymer Submicrospheres, *J. Mater. Chem.*, 2010, **20**, 5493-5498.
56. E. J. Moon, P. Sonveaux, P. E. Porporato, P. Danhier, B. Gallez, I. Batinic-Haberle, Y. C. Nien, T. Schroeder and M. W. Dewhirst, NADPH Oxidase-Mediated Reactive Oxygen Species Production Activates Hypoxia-Inducible Factor-1 (HIF-1) via the ERK Pathway After Hyperthermia Treatment, *Proc. Natl. Acad. Sci. U. S. A.*, 2010, **107**, 20477-20482.
57. Z. C. Wang, F. Cai, X. Y. Chen, M. H. Luo, L. L. Hu and Y. Lu, The Role of Mitochondria-Derived Reactive Oxygen Species in Hyperthermia-Induced Platelet Apoptosis, *PLoS One*, 2013, **8**, e75044.
58. K. Hayashi, M. Moriya, W. Sakamoto and T. Yogo, Chemoselective Synthesis of Folic Acid-Functionalized Magnetite Nanoparticles via Click Chemistry for Magnetic Hyperthermia, *Chem. Mat.*, 2009, **21**, 1318-1325.

Graphical Abstract

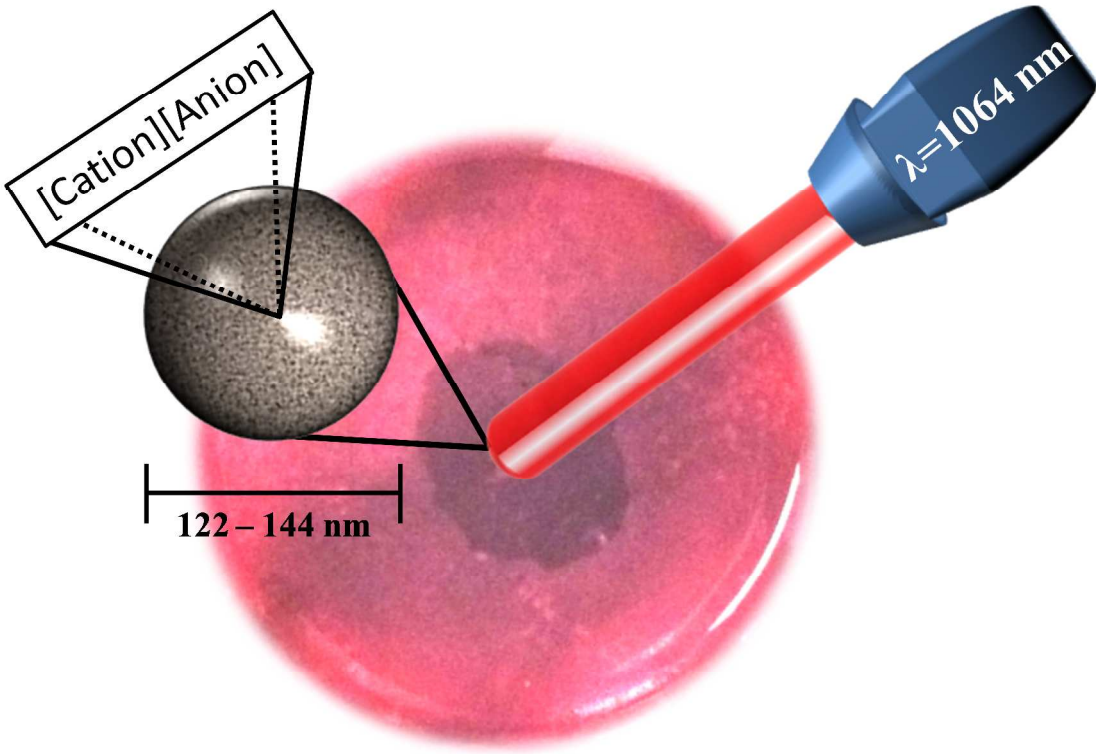

Nanoparticles devised entirely of ionic liquid-like materials called GUMBOS created a localized hyperthermal effect within breast cancer cells concurrent with near-infrared laser excitation.